THE JOURNAL OF PHYSICAL CHEMISTRY B

Article

pubs.acs.org/JPCB

Hydroxyl-Proton Hydrogen Bonding in the Heparin Oligosaccharide Arixtra in Aqueous Solution

Consuelo N. Beecher, Robert P. Young, Derek J. Langeslay, Leonard J. Mueller,* and Cynthia K. Larive*

Department of Chemistry, University of California−Riverside, Riverside, California 92521, United States

Supporting Information

ABSTRACT: Heparin is best known for its anticoagulant activity, which is mediated by the binding of a specific pentasaccharide sequence to the protease inhibitor antithrombin-III (AT-III). Although heparin oligosaccharides are thought to be flexible in aqueous solution, the recent discovery of a hydrogen bond between the sulfamate ($NHSO_3^-$) proton and the adjacent 3-*O*-sulfo group of the 3,6-*O*-sulfated *N*-sulfoglucosamine residue of the Arixtra (fondaparinux sodium) pentasaccharide demonstrates that definable elements of local structure are accessed. Molecular dynamics simulations of Arixtra suggest the presence of additional hydrogen bonds involving the C3-OH groups of the glucuronic acid and 2-*O*-sulfo-iduronic acid residues. NMR measurements of temperature coefficients, chemical shift differences, and solvent exchange rate constants provide experimental confirmation of these hydrogen bonds. We note that the extraction of rate constants from cross-peak buildup curves in 2D exchange spectroscopy is complicated by the presence of radiation damping in aqueous solution. A straightforward model is presented that explicitly takes into account the effects of radiation damping on the water proton relaxation and is sufficiently robust to provide an accurate measure of the proton exchange rate between the analyte hydroxyl protons and water.

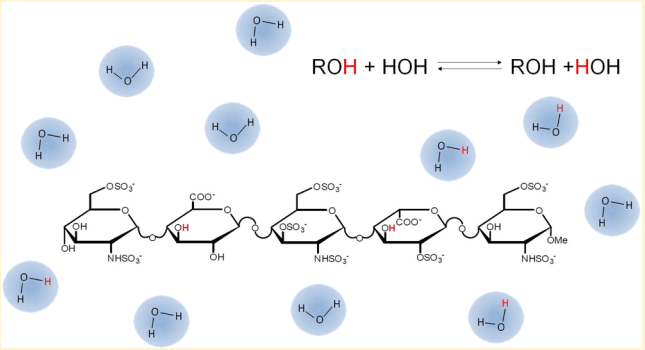

INTRODUCTION

Heparin is an unbranched, anionic, linear polysaccharide and a member of the glycosaminoglycan (GAG) family that is synthesized in the endoplasmic reticulum and Golgi apparatus of mast cells.[1] Although the basic structure of heparin consists of repeating (1 → 4)-linked uronic acid−glucosamine disaccharides, microheterogeneity is introduced by various patterns of sulfation and epimerization, resulting in the presence of both L-iduronic (IdoA) and D-glucuronic acid (GlcA) C5 epimers.[2] As a result of this intricacy, it is not currently possible to define the primary structure of intact heparin. Enzymatic or chemical depolymerization reactions are typically used to reduce heparin to variously sized oligosaccharides for its clinical use as low-molecular-weight heparin (LWMH) or for fractionation and molecular-level characterization by nuclear magnetic resonance (NMR) spectroscopy and mass spectrometry (MS).[3]

Heparin exhibits a variety of biological effects including inhibition of angiogenesis and tumor growth through well-characterized interactions with fibroblast growth factors (FGFs),[4−6] vascular endothelial growth factor (VEGF),[7−9] lipases,[10−12] and cytokines,[13−15] but it is best known for its role as an anticoagulant and antithrombotic, acting by binding to the protease inhibitor antithrombin-III (AT-III).[16,17] The anticoagulant activity of heparin has been studied extensively, and the structure of the native pentasaccharide sequence responsible for high-affinity AT-III binding is known.[18] A synthetic pentasaccharide that mimics this binding sequence is currently used clinically and marketed as Arixtra (fondaparinux sodium). A critical structural element of the AT-III binding pentasaccharide is the internal 3,6-*O*-sulfated *N*-sulfoglucosamine (GlcNS3S6S) residue. Removal of the 3-*O*-sulfo moiety decreases the affinity of the pentasaccharide for AT-III by 1000-fold.[19] The conformational flexibility of the 2-*O*-sulfated iduronic acid (IdoA2S) residue of the pentasaccharide is also important for AT-III binding. The IdoA2S residue can exist in two different conformations: chair ($^1C_4$) and skew boat (^2S_O), which interconvert at a rate that is fast on the NMR time scale. In oligosaccharides in which the IdoA2S residue is connected to a 6-*O*-sulfated GlcNS residue at its nonreducing end, the equilibrium slightly favors the $^1C_4$ conformer ($^1C_4/^2S_O$ = 60:40). If this GlcNS residue is 3,6-*O*-sulfated, however, equilibrium of the adjacent IdoA2S shifts to favor the ^2S_O conformer (>60%).[20] In the AT-III complex, however, the IdoA2S residue of the pentasaccharide is exclusively in the ^2S_O conformation, causing the "kink" observed in the otherwise linear oligosaccharide chain.[21] The 6-*O*-sulfo group at the nonreducing end GlcNS6S residue of the pentasaccharide also contributes to its AT-III binding affinity and in the crystal structure is involved in a hydrogen bond to the side chain of Arg129.[22] Although the glucuronic acid (GlcA) residue of the pentasaccharide has been reported to be neutral with respect to

Received: October 24, 2013
Revised: December 18, 2013
Published: December 19, 2013

ACS Publications © 2013 American Chemical Society

the binding energy,[19] the crystal structure reveals a hydrogen bond between the GlcA carboxylate moiety and the side chain of Lys125, as well as a salt bridge with Asn45.[22]

Understanding how elements of local structure impact the solution conformation of heparin oligosaccharides can potentially provide insights into the nature of heparin−protein interactions. Although oligosaccharides are thought to be flexible in solution, specific structural motifs might favor formation of intramolecular hydrogen bonds that restrict the conformation and preorganize a local structure for high-affinity protein binding. For example, we recently identified a persistent hydrogen bond involving the Arixtra GlcNS3S6S sulfamate NH through ^{1}H NMR spectra examining the pH and temperature dependence of the $NHSO_3^-$ resonances in a series of heparin oligosaccharides.[23] Molecular dynamics simulations suggested the presence of this hydrogen bond in both IdoA2S conformations of Arixtra and identified the hydrogen-bond acceptor as the adjacent 3-*O*-sulfo group.[23] Our molecular dynamics simulations also predicted that additional intramolecular hydrogen bonds involving the Arixtra hydroxyl protons could further stabilize its secondary structure, a possibility explored experimentally in this study.

Several experimental strategies have been used to quantitatively assess hydroxyl-proton hydrogen bonding in aqueous solutions of oligosaccharides. Small hydroxyl-proton temperature coefficients (the slope of the chemical shift with temperature) suggest protection from exchange with water, most likely by participation in a hydrogen bond, although chemical shift changes can also arise from temperature-dependent conformational changes. Differences in the hydroxyl-proton chemical shift compared to their corresponding monosaccharide values ($\Delta\delta = \delta_{oligo} - \delta_{mono}$) can also be diagnostic of hydrogen bonding.[24] A positive $\Delta\delta$ value suggests additional hydration from other exchangeable protons, whereas a negative $\Delta\delta$ value indicates close spatial proximity of the hydroxyl proton to an electronegative atom, as would be expected in a hydrogen bond.[25] For example, through analysis of temperature coefficients, $\Delta\delta$ values, and rotating-frame nuclear Overhauser effect spectroscopy (ROESY) cross-peaks, Vilen et al. identified hydroxyl-proton hydrogen bonds in κ-/μ-hybrid carrageenan that are absent in the structurally related κ-carrageenan oligosaccharides.[24] Chemical shift differences can also result from isotope effects, which the O'Leary group used to determine the presence of hydrogen bonds in partially deuterated diols.[26]

Results of similar studies for sucrose have been more controversial. For example, Adams and Lerner evaluated sucrose in water/acetone solution using hydroxyl-proton temperature coefficients, coupling constants, and solvent exchange rates and concluded that intramolecular hydrogen bonds were not sufficiently persistent to be detected by NMR spectroscopy.[27] Poppe and van Halbeek also studied sucrose in water/acetone solution, detecting interresidue NOE contacts and OH−OH ROESY chemical exchange peaks consistent with a hydrogen bond between the glucose OH2 and the fructose OH1. Although their results supported the persistence of the interresidue hydrogen bond detected in the sucrose crystal structure, Poppe and van Halbeek concluded that, in solution, sucrose does not behave as a rigid body but has a high degree of internal flexibility.[28] Recently, Battistel et al. reported the results of NMR studies in supercooled aqueous solutions of sucrose at high concentrations (e.g., 300 mM). The ^{13}C heteronuclear single quantum correlation (HSQC)−total correlation spectroscopy (TOCSY) experiment was used to directly detect interresidue cross-peaks indicative of hydroxyl hydrogen bonds, which were confirmed by $^{2}J_{OH-OH}$ coupling detected in the correlation spectroscopy (COSY) spectrum.[29] Molecular dynamics (MD) simulations and diffusion-ordered spectroscopy (DOSY) experiments were used to discriminate intramolecular hydrogen bonding from possible aggregation-induced intermolecular hydrogen bonds. The Freedberg group used a similar experimental strategy to directly detect patterns of hydrogen bonding in a ^{15}N,^{13}C-labeled α2-8 sialic acid tetramer, providing direct evidence of hydrogen bonding through a CBCANH NMR experiment.[30]

Inspired by recent reports of hydrogen bonding in oligosaccharides[24,25,29,31] and motivated by our prior molecular dynamics study,[23] we embarked on an investigation of hydroxyl-group hydrogen bonding in aqueous solutions of Arixtra. The limited quantity of Arixtra available and the necessity of performing the measurements without the benefit of ^{13}C and ^{15}N isotopic enrichment precluded the direct detection of hydrogen bonds as described by Battistel et al.[29,30] In addition, in heparin oligosaccharides, we anticipate OH hydrogen bonding through *N*- or *O*-sulfate groups, which would be challenging to detect through long-range couplings, especially at the natural abundance levels of ^{15}N and ^{13}C.

In this work, ^{1}H NMR experiments were performed to evaluate temperature coefficients, differences in hydroxyl-proton chemical shifts relative to their monosaccharide values, and solvent exchange rates for Arixtra in aqueous solution. To accomplish our experimental objectives, the contribution of water radiation damping in the exchange rate calculations was also addressed. To our knowledge, this study provides the first experimental evidence of solution state hydrogen bonds involving the hydroxyl protons of a heparin oligosaccharide.

The quantification of hydroxyl proton−solvent exchange rates through measurement of cross-peak intensity in two-dimensional chemical exchange spectroscopy (EXSY) spectra acquired as a function of mixing time can provide evidence for the involvement of a hydroxyl proton in a hydrogen bond.[31,32] A lower rate of increase (or buildup) of EXSY cross-peak intensity indicates that a hydroxyl proton is protected from exchange with water, as would be the case under hydrogen bonding. In aqueous solution, radiation damping induced by water magnetization makes a significant contribution to the observed longitudinal relaxation of the hydroxyl protons. The observed magnetization dynamics of water and exchanging protons is governed by a radiation-damped relaxation mechanism described by Chen and Mao for the exchange of the NH protons of guanidine chloride with water.[33] Therefore, a challenge in interpreting the results of EXSY measurements for dilute aqueous solutions of heparin oligosaccharides is that analysis of the hydroxyl-proton buildup curves must consider both the contribution from radiation damping and the hydroxyl-proton T_1 relaxation rates. Here, we adapt the radiation-damped exchange model of Chen and Mao to the case of 2D EXSY correlation spectroscopy. Although radiation damping complicates the analysis, quantitative determination of the exchange rates is accomplished in a robust manner.

EXPERIMENTAL SECTION

Materials and Reagents. Arixtra (fondaparinux sodium), formulated as prefilled syringes for clinical use, was obtained from the University Pharmacy and Department of Pharmacy Administration of Semmelweis University (Budapest, Hungary). 2,2-Dimethyl-2-silapentane-5-sulfonate-d_6 sodium salt (DSS) and the GlcNS6S and D-GlcA monosaccharides were purchased from Sigma-Aldrich (Saint Louis, MO). High-performance-liquid-chromatography- (HPLC-) grade water was obtained

dx.doi.org/10.1021/jp410540d | J. Phys. Chem. B 2014, 118, 482−491

from Burdick and Jackson (Muskegon, MI). Acetone-d_6 (99.9% D), deuterium oxide (99.9% D), deuterated hydrochloric acid, and sodium deuteroxide were purchased from Cambridge Isotope Laboratories (Andover, MA). The pH meter was calibrated with buffers of 4.00, 7.00, and 10.00 purchased from Fisher Scientific.

MD Simulations. The combined results of hydrogen-bonding analyses of five molecular dynamics (MD) simulations of Arixtra in explicit solvent are reported. One 5-ns MD simulation was previously described in Langeslay et al.,[23] and the results were combined with the four additional simulations described herein. The initial heavy-atom coordinates for two of the four additional simulations, 6 and 75 ns in duration, were extracted from the X-ray crystal structure of the bound pentasaccharide with Antithrombin-S195A factor Xa [Protein Data Bank (PDB) ID 2GD4].[22] The final two simulations were initiated from starting coordinates better approximating the solution conformation of Arixtra by extracting structures from individual frames of the first MD run. These included one of each observed conformation of the IdoA2S residue, $^1C_4$ and ^2S_O, and were additionally modified by adjusting the interglycosidic dihedral angles φ_H (H1−C1−O1−C4′) and ψ_H (C1−O1−C4′−H4′) to the same values listed as the free-state averages by Hricovini et al. using the VEGA ZZ program.[21,34] The last two simulations were 9.3 ns in duration. Table S1 in the Supporting Information lists the average φ_H and ψ_H dihedral angles measured during each trajectory. The AmberTools 11 xleap module was used to parametrize Arixtra with the GLYCAM06g force field to neutralize the system charge by adding sodium ions (ff99SB force field) and to construct a rectangular water box of TIP3P-parametrized water molecules with faces extending at least 12 Å from the solute.[35−38]

NAMD 2.8 was used to calculate all minimization, heating, equilibration, and production trajectories.[39] Conjugate-gradient minimization was applied to the solvent, solutes, and finally the entire system to remove bad contacts. The system was heated slowly in the constant-*NVE* ensemble from 0 to 298 K in 398 ps, including a 100-ps hold at the target temperature. Equilibration and production runs were conducted in the constant-*NPT* ensemble with a pressure of 1 atm and a temperature of 298 K. The temperature was maintained using the Langevin thermostat with a damping coefficient of 5 ps^{-1}, and the pressure was controlled by NAMD's Nosé−Hoover Langevin piston method.[39] The nonbonded interactions were cut off at 12 Å with a smooth switching function applied at 10 Å. The van der Waals and electrostatic 1−4 scaling factors were set to unity for consistency with the GLYCAM06g parametrization.[36] Periodic boundary conditions were applied throughout, and the particle mesh Ewald summation was employed to handle long-range electrostatics with a grid spacing of 1 Å.[40] Only the hydrogen−oxygen bonds within water molecules were held rigid using the SETTLE algorithm.[41] All simulations were integrated in 1-fs time steps. The trajectory output was saved every 1000 fs for the 75-ns-duration simulation and every 100 fs for all other simulations. VMD 1.9 was used for the visualization of trajectories, as well as the monitoring of temperature, pressure, and energy data.[42] The AmberTools 11 ptraj module was used to compute dihedral angles and interatomic distances and to analyze hydrogen bonding.[35] The hydrogen-bonding analysis included a 3.5-Å heavy-atom cutoff distance and a 120° angle cutoff. Forster's mdxvu program was used to compute and monitor the Cremer−Pople ring-puckering parameters of all five rings over the course of the simulation production runs.[43] In three of the five simulations, the IdoA2S residue was observed to transition between the ^2S_O and $^1C_4$ conformations. The trajectories in which this occurred were divided according to IdoA2S conformation, and the periods corresponding to the transitions, which took place in less than 14 ps each, were excluded from the hydrogen-bonding analyses. Plots of the Cremer−Pople θ parameter versus time for each monomer and histograms of the φ_2 parameter for the IdoA2S residue when in the ^2S_O conformation are included in the Supporting Information as Figure S1. The results of the hydrogen-bonding analyses per IdoA2S conformation were then weighted by frames and averaged. In terms of frames from the resulting MD trajectories, the population ratio of ^2S_O to $^1C_4$ conformers observed for the IdoA2S residue was approximately 50:50. Experimental studies of Arixtra in solution indicated that the ratio of IdoA2S conformations best satisfying observed $^3J_{HH}$ coupling constants is approximately 60:40 ($^2S_O/^1C_4$).[44,45] The results of the hydrogen-bonding analysis indicated that some hydrogen bonds are affected by the conformation of the IdoA2S residue, and therefore, to compute overall average hydrogen-bond occupancy percentages, the weights of 60:40 $^2S_O/^1C_4$ were applied.

NMR Measurements of the Arixtra OH Resonances. To reduce the solvent exchange rate of the hydroxyl protons, Arixtra and monosaccharide NMR samples were prepared at concentrations of 1−2 mM in a CO_2-free environment and studied at reduced temperatures in 85% H_2O/15% acetone-d_6 containing 0.15 M NaCl.[24,27] Spectra were recorded as a function of pH (Figure S2, Supporting Information) using dilute solutions of CO_2-free HCl and NaOH, and the pH was set to 8.1 for subsequent measurements. Solution pH measurements were made prior to the addition of acetone-d_6 using a Fisher Scientific AB15 pH meter with a double-junction Ag/AgCl micro-pH electrode (Thermo Scientific, Beverly, MA). NMR measurements were performed in 5-mm NMR tubes using a 600-μL sample.

Solvent suppression was accomplished using excitation sculpting to avoid the signal attenuation often observed with WATERGATE.[46] Hydroxyl-proton resonances were assigned using the two-dimensional COSY (Figure S3A, Supporting Information) and TOCSY (Figure S3B, Supporting Information) NMR spectra at −14.5 °C using a Bruker 600 MHz Avance spectrometer equipped with a triple inverse gradient (TXI) probe operating at 600.13 MHz.[47] Temperature coefficients were measured by recording ^{1}H NMR spectra over the temperature range from −14.5 to 11.5 °C in approximately 4−5 °C increments. The temperature was calibrated using an external methanol standard.[48] Chemical shifts were referenced using the residual ^{1}H resonance of acetone-d_6 at 2.204 ppm. The $\Delta\delta$ values for each monosaccharide were determined at −10.0 °C. Experimental details and chemical shift assignments are reported in the Supporting Information.

EXSY spectra were acquired using the Bruker NOESY pulse program "noesyesgpph" at −14.5 °C using excitation-sculpting solvent suppression and mixing times ranging from 0 to 24 ms in 3-ms increments. Two thousand forty-eight complex-valued time-domain points in t_2 and 128 complex time-domain points in t_1 were acquired using a relaxation delay of 1.5 s and the coaddition of 32 scans per t_1 increment. A spectral window of 4440 Hz was used in both F1 and F2 frequency domains. The spectra were zero-filled to 16384 × 4096 points to obtain more accurate volume integrals of the hydroxyl cross-peaks and apodized using a cosine function. Buildup curves were plotted as volume integrals of the hydroxyl-exchange cross-peaks as a

dx.doi.org/10.1021/jp410540d | J. Phys. Chem. B 2014, 118, 482−491

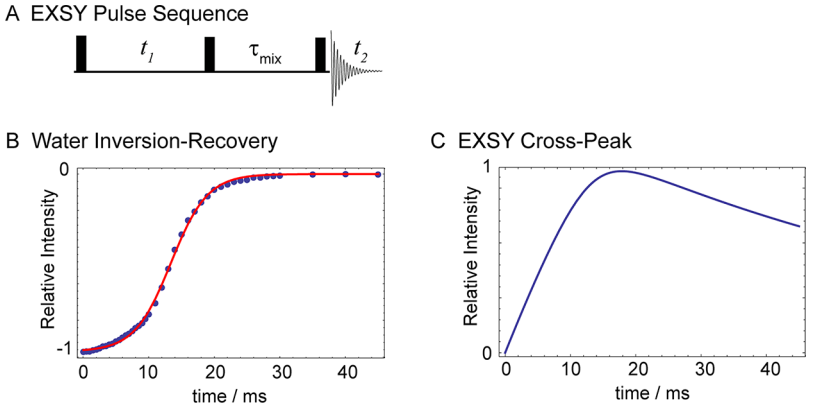

Figure 1. (A) Pulse sequence for 2D exchange correlation spectroscopy (EXSY). (B) Inversion recovery of water magnetization performed and phase cycled using the EXSY pulse sequence with $t_1 = 0$ and τ_{mix} varied. The blue data points were fit by eq 2 to give $T_{RD} = 5.5$ ms and $t_0 = 13.4$ ms. (C) Intensity predicted from eq 5 for a cross-peak between water (subject to radiation damping with $T_{RD} = 5.5$ ms and $t_0 = 13.4$ ms) and an analyte with $k = 15$ s^{-1}.

function of mixing time. The cross-peak volume integrals were measured using the TopSpin integration program and normalized to the diagonal peak for each resonance. In cases where peaks were slightly overlapped, the volume was determined only for the portion of the cross-peak that was well-resolved. To provide consistency, the same chemical-shift regions were used for cross-peak volume integration in each experiment. Initial rate constants were calculated from the EXSY data using modified Bloch equations to include chemical exchange and relaxation time of the water governed by radiation damping as discussed below.[32,33]

Proton Exchange with Solvent in the Presence of Radiation Damping. In 2D exchange correlation spectroscopy (Figure 1A),[49] the cross-peak intensity shows a time response that depends on the exchange rate and the spin relaxation properties. For analyte protons undergoing exchange with water in aqueous solution, this process is complicated by radiation damping, the significantly enhanced drive to equilibrium for intense resonances in highly concentrated solutions.[33,50−53] In radiation damping, a large transverse sample magnetization induces a substantial signal voltage across the detection coil, which in turn generates a magnetic "reaction" field 90° out of phase with the transverse component, rotating it back toward alignment with the field in a nearly selective manner. Because of this, proton spins in water do not relax exponentially, but rather relax with a rate proportional to their transverse magnetization, complicating the analysis of EXSY cross-peaks.

Chen and Mao demonstrated that quantitative analysis of exchange is still possible (and is in some ways enhanced) under radiation damping.[33,53] Here, we adapt their analysis to the problem of cross-peak intensity in EXSY experiments. The cross-peak of interest is that from water to the analyte, and in our experiments the water is placed on resonance—a requirement in the analysis that follows, which assumes that the bulk water magnetization is aligned either parallel or antiparallel to the magnetic field at the start of τ_{mix}. Indeed, to suppress zero-frequency artifacts in the indirect dimension (due to relaxation during t_1 and τ_{mix}), standard phase cycling in EXSY experiments alternately places the water magnetization along and against the field, with a corresponding 180° phase shift of the receiver.[54] For full inversion of the water resonance, the z magnetization recovers under radiation damping according to the expression

$$M_{H_2O,z}(t) = M^{o}_{H_2O,z} \tanh[(t - t_0)/T_{RD}] \quad (1)$$

where $M^{o}_{H_2O,z}$ is the net equilibrium magnetization, $1/T_{RD}$ is the radiation-damping rate constant, t_0 is the latency interval that is related to the initial angular deviation of the inversion from 180°, and T_1 relaxation of water is ignored.[52] When the magnetization is placed in alignment with the field, the radiation-damping mechanism is not operative, and the bulk magnetization persists. Thus, the net water decay in the EXSY experiment has the form

$$M_{H_2O,z}(t) = M^{o}_{H_2O,z} \{\tanh[(t - t_0)/T_{RD}] - 1\}/2 \quad (2)$$

Figure 1B shows a simple inversion-recovery experiment, phase cycled as described above and using the pulse sequence shown with $t_1 = 0$. This signal is fit well by eq 2 with $T_{RD} = 5.5$ ms and $t_0 = 13.4$ ms.

During the mixing time of an EXSY experiment, protons exchange between water and the analyte. Because of the vastly different concentrations of the analyte (<2 mM) and water (55 M × 2 protons per water molecule), exchange with the analyte does not significantly perturb the water magnetization, and eq 2 continues to be an excellent model for the water nuclear spin magnetization. The buildup of cross-peak intensity from water to the analyte can then be written as

$$\begin{aligned}\frac{dM_{analyte,z}(t)}{dt} &= -kM_{analyte,z}(t) - \frac{M_{analyte,z}(t)}{T_1} + kX_{analyte}\frac{M_{H_2O,z}(t)}{2} \\ &= -kM_{analyte,z}(t) - \frac{M_{analyte,z}(t)}{T_1} + \frac{kX_{analyte}M^{o}_{H_2O,z}}{4}\{\tanh[(t - t_0)/T_{RD}] - 1\} \\ &= -kM_{analyte,z}(t) - \frac{M_{analyte,z}(t)}{T_1} + \frac{kM^{o}_{analyte,z}}{2}\{\tanh[(t - t_0)/T_{RD}] - 1\}\end{aligned} \quad (3)$$

where k is the proton exchange rate from the analyte to water, $X_{analyte}$ is the mole fraction of analyte (note that $kM^{o}_{analyte,z} = kX_{analyte}\, M^{o}_{H_2O,z}/2$ follows from detailed balance), and $1/T_1$ is the analyte longitudinal relaxation rate. This equation can be integrated (performed here within Mathematica[55]) subject to the cross-peak initial condition, $M_{analyte,z}(0) = 0$, to give a closed-form

dx.doi.org/10.1021/jp410540d | J. Phys. Chem. B 2014, 118, 482−491

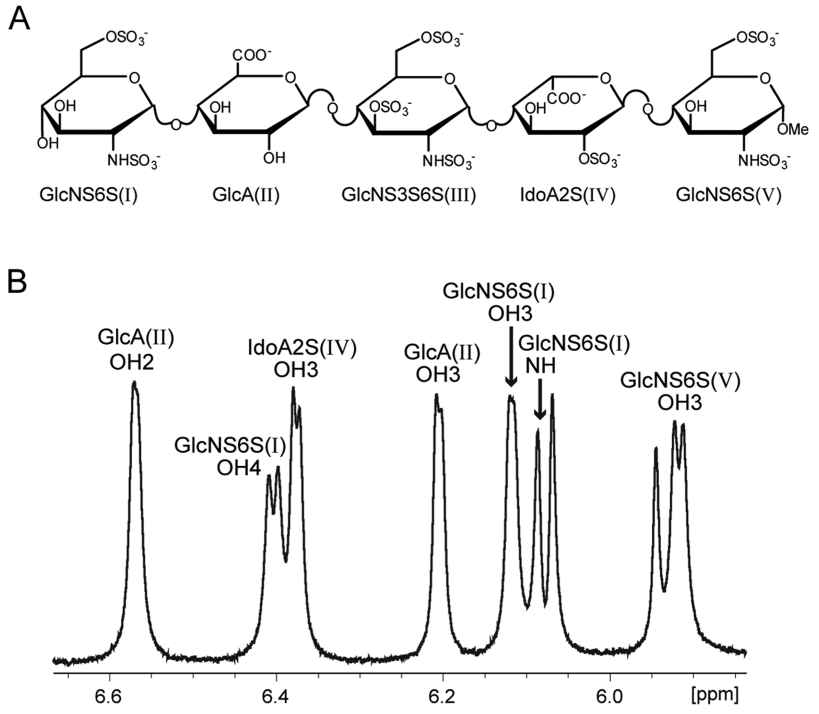

Figure 2. (A) Structure of Arixtra with residues labeled. (B) ^{1}H NMR spectrum of Arixtra measured in 85% H_2O/15% acetone-d_6 at pH 8.1 and −14.5 °C with hydroxyl and sulfamate proton resonances indicated.

solution in terms of the generalized hypergeometric function ${}_2F_1(a,b;c;x)$[56]

$$\frac{M_{\text{analyte},z}(t)}{M^{\circ}_{\text{analyte},z}} = \frac{[1 - e^{-(k+1/T_1)t}]kT_1}{1 + kT_1} - \frac{e^{2(t-t_0)/T_{RD}}kT_1}{1 + kT_1 + 2T_1/T_{RD}} \times {}_2F_1\left(1, \frac{1 + kT_1 + 2T_1/T_{RD}}{2T_1/T_{RD}}; \frac{1 + kT_1 + 4T_1/T_{RD}}{2T_1/T_{RD}}; -e^{2(t-t_0)/T_{RD}}\right) + \frac{e^{-(k+1/T_1)t-2t_0/T_{RD}}kT_1}{1 + kT_1 + 2T_1/T_{RD}} \times {}_2F_1\left(1, \frac{1 + kT_1 + 2T_1/T_{RD}}{2T_1/T_{RD}}; \frac{1 + kT_1 + 4T_1/T_{RD}}{2T_1/T_{RD}}; -e^{-2t_0/T_{RD}}\right) \quad (4)$$

One additional approximation that is typically valid for small molecules is that the longitudinal relaxation time of the analyte is much longer than T_{RD} and $1/k$, allowing eq 4 to be written as

$$\frac{M_{\text{analyte},z}(t)}{M^{\circ}_{\text{analyte},z}} = 1 - e^{-kt} - \frac{e^{2(t-t_0)/T_{RD}}k}{k + 2/T_{RD}} \times {}_2F_1\left(1, \frac{2 + kT_{RD}}{2}; \frac{4 + kT_{RD}}{2}; -e^{2(t-t_0)/T_{RD}}\right) + \frac{e^{-kt-2t_0/T_{RD}}k}{k + 2/T_{RD}} {}_2F_1\left(1, \frac{2 + kT_{RD}}{2}; \frac{4 + kT_{RD}}{2}; -e^{-2t_0/T_{RD}}\right) \quad (5)$$

In the fits described below, we found negligible differences in the extracted rate constants k and radiation-damping parameters T_{RD} and t_0 using either eq 4 or eq 5, with nearly identical qualities of fit.

As an example, Figure 1C shows the predicted time response of the cross-peak intensity using the radiation-damping parameters from Figure 1B and an exchange rate of 15 s^{-1}. Initially, radiation damping is slow, and the cross-peak intensity increases with a rate of

$$\frac{d}{dt}\left(\frac{M_{\text{analyte},z}(t)}{M^{\circ}_{\text{analyte},z}}\right)_{t=0} = \frac{k}{2}\{1 + \tanh[t_0/T_{RD}]\} \approx k \quad (6)$$

However, a characteristic of radiation damping is that the solvent magnetization quickly transitions from full polarization to zero between times $t_0 - T_{RD}$ and $t_0 + T_{RD}$. This rapid depletion of source magnetization coincides with the cross-peak reaching its maximum intensity and then decaying exponentially under the influence of exchange and T_1. At first sight, radiation damping might seem to complicate the analysis of exchange, but upon further examination, the switching off of the solvent magnetization and subsequent free decay of the analyte magnetization provides a robust mechanism for segregating the effect of exchange and the relaxation properties of water and the analyte. The process of extracting the exchange rate is made even more straightforward if an independent measurement of T_{RD} and t_0 is made, as we do below for the sample mixtures of Arixtra in water.

RESULTS AND DISCUSSION

To investigate experimentally the occurrence of the hydroxyl hydrogen bonds predicted by our MD simulations, Arixtra hydroxyl-proton resonance temperature coefficients, chemical shift differences, and relative rates of chemical exchange with water were compared. The hydroxyl resonances were observed to be most intense over the pH range of 7.8−8.8 (Figure S2, Supporting Information), which is consistent with the optimum conditions for measurement of the Arixtra exchangeable NH resonances of the GlcNS sulfamate ($NHSO_3^-$) groups.[23,57,58] Samples were prepared under nitrogen atmosphere to avoid catalysis of proton exchange by dissolved carbon dioxide.[27,31] Addition of 0.15 M NaCl was found to enhance the stability of the pH measurements and the reproducibility of the spectral measurements.

The use of excitation sculpting for solvent suppression allows detection of exchangeable protons by NMR spectroscopy.[46]

dx.doi.org/10.1021/jp410540d | J. Phys. Chem. B 2014, 118, 482−491

Table 1. Combined Results of MD Hydrogen-Bonding Analyses as Percentages of Frames Occupied by IdoA2S Residue Conformation and Overall[a]

donor	acceptor	^2S_O	$^1C_4$	overall[b]
GlcA(II) 3OH	GlcNS6S(I) 2-*N*-sulfo	85	92	88
GlcNS3S6S(III) 2NH	GlcNS3S6S(III) 3-*O*-sulfo	89	63	79
IdoA(IV) 3OH	GlcNS3S6S(III) *N*-sulfo	35	2	22
IdoA(IV) 3OH	IdoA2S(IV) 2-*O*-sulfo	49	0	29
GlcNS6S(V) 3OH	IdoA(IV) O5 (ring oxygen)	32	60	43

[a]Only hydrogen bonds with percentage occupancies of greater than 20% for either conformation are listed. [b]Weighted 60% ^2S_O and 40% $^1C_4$.

In this case, the suppression of the solvent resonance is applied directly after the mixing period in Figure 1A. To further reduce the rate of hydroxyl-proton exchange with water, spectra were acquired at −14.5 °C, requiring addition of 15% acetone-d_6 to avoid freezing the sample. Adams and Lerner demonstrated that a low concentration of acetone does not significantly affect the relative temperature coefficients and exchange rates of sugar hydroxyl protons.[27,28] It should also be noted, however, that chemical exchange is strongly influenced by solution composition, pH, and temperature. The structure of Arixtra with its residues labeled is shown in Figure 2A. The position of the individual monosaccharide residues within the oligosaccharide is indicated by a Roman numeral, starting from the nonreducing end. There are a total of six hydroxyl protons, each in a different chemical environment. Visual examination of Figure 2B reveals differences in the line widths of the Arixtra hydroxyl protons. For some protons, the resonances are sufficiently sharp that even small couplings are resolved, whereas other peaks are broader, suggesting differences in the solvent exchange rate within a given oligosaccharide.

MD Simulations. The results of the hydrogen-bonding analyses of the five MD simulations are summarized in Table 1 and Figure 3 as the percentages of frames in which the given hydrogen bonds were detected. Only hydrogen bonds detected at greater than 20% occupancy for either conformation are listed in the table. Although numerous intramolecular hydrogen bonds were detected, only four hydrogen-bond donors, GlcA(II) 3OH, GlcNS3S6S(III) 2NH, IdoA2S(IV) 3OH, and GlcNS6S(V) 3OH, were consistently involved in hydrogen bonds with an overall combined percentage occupancy of greater than 40%. The next highest occupancy was 12%. The IdoA2S(IV) 3OH was observed to alternate its hydrogen-bond donation between the GlcNS3S6S(III) 2-sulfamate oxygen atoms and the IdoA2S(IV) 2-sulfo oxygen atoms when in the ^2S_O conformation so that, when weighted 60% ^2S_O and 40% $^1C_4$, an overall occupancy of 51% still resulted.

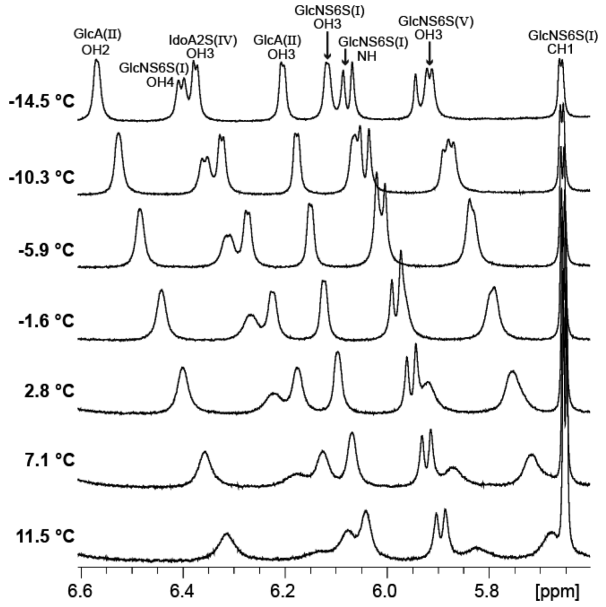

Figure 4. Exchangeable hydroxyl and sulfamate proton resonances of Arixtra experience a linear shift toward the water resonance as the temperature increases, whereas the resonances of the carbon-bound protons are unaffected. Exchange broadening of the hydroxyl-proton resonances is also observed as the temperature is increased.

Hydroxyl-Proton Temperature Coefficients (Δδ/ΔT). The temperature dependence of the ^{1}H NMR resonances of exchangeable protons can provide a qualitative indication of hydrogen bonding.[27,59−61] As illustrated in Figure 4, the Arixtra hydroxyl resonances broaden and shift linearly upfield as the

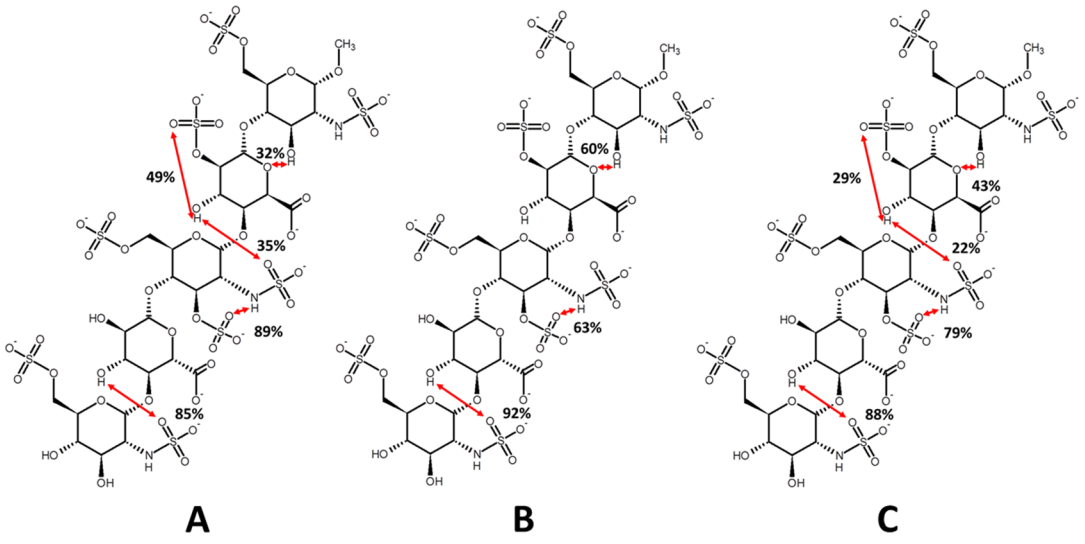

Figure 3. Graphical depiction of intramolecular hydrogen bonding predicted from MD simulations of Arixtra as percentage lifetime of frames occupied by the IdoA2S residue conformations (A) ^2S_O, (B) $^1C_4$, and (C) overall (weighted 60% ^2S_O and 40% $^1C_4$). Only hydrogen bonds with percentage occupancies greater than 20% are depicted.

dx.doi.org/10.1021/jp410540d | J. Phys. Chem. B 2014, 118, 482−491

Table 2. Chemical Shift Differences, Temperature Coefficients, and Exchange Rate Constants of the Arixtra Hydroxyl Protons

residue	hydroxyl proton	temperature coefficient (ppb/K)	$\Delta\delta$ (ppm)	initial buildup rate (k_{ex}, s^{-1})
GlcNS6S(I)	OH3	11.2	−0.008	13.8
GlcNS6S(I)	OH4	10.5	−0.160	14.2
GlcA(II)	OH2	9.9	−0.006	22.6
GlcA(II)	OH3	6.4	−0.278	4.72
IdoA2S(IV)	OH3	11.4	N/A[a]	5.73
GlcNS6S(V)	OH3	9.1	−0.199	25.9

[a]Result not available.

temperature is increased. Visual inspection of the spectra in Figure 4 shows differences in the extent of line broadening as the temperature is raised. The line widths of the IdoA2S(IV) OH3 and GlcA(II) OH3 resonances increase more gradually than those of the other OH resonances as the temperature increases. The temperature coefficients, calculated as the change in chemical shift as a function of temperature, are summarized in Table 2. The GlcA(II) OH3 resonance has the smallest temperature coefficient, 6.4 ppb/K, with the other hydroxyl resonances producing temperature coefficients greater than 9 ppb/K. This result suggests a qualitatively different environment for the GlcA(II) OH3, consistent with the results of the molecular dynamics simulation (Figure 3), which showed this OH group to be involved in a persistent hydrogen bond with the GlcNS6S(I) sulfamate group. Although the MD simulations also predict a hydrogen bond 51% of the time for the IdoA2S(IV) OH3 hydroxyl proton, this is not reflected in the temperature coefficient measured for this resonance. The MD simulation suggests that the IdoA2S(IV) OH3 hydrogen bond alternates between two different sulfate groups, which could be responsible for the larger temperature coefficient (11.4 ppb/K) of this resonance.

Chemical Shift Differences ($\Delta\delta$). A large negative deviation in the chemical shift of an oligosaccharide hydroxyl-proton resonance relative to is value in the corresponding monosaccharide can be indicative of close spatial proximity to an electronegative atom, as expected in a hydrogen bond.[24,25] The $\Delta\delta$ ($\Delta\delta = \delta_{oligo} - \delta_{mono}$) values of the hydroxyl protons in each Arixtra residue are summarized in Table 2. Unfortunately, the IdoA2S monosaccharide was unavailable, so the chemical-shift comparison for this residue is omitted from Table 2. In Arixtra, the GlcA(II) OH3 has the

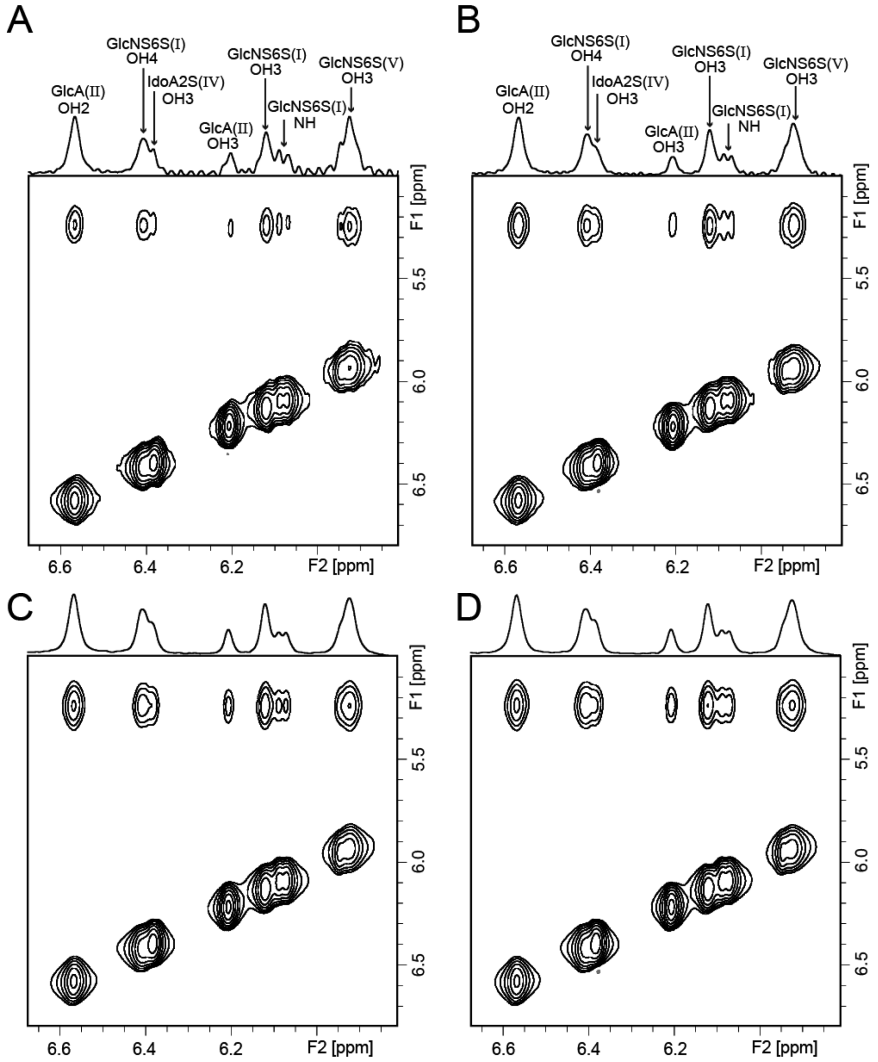

Figure 5. EXSY spectra of Arixtra at mixing times of (A) 6, (B) 12, (C) 18, and (D) 24 ms showing differences in the exchange cross-peak intensity of each hydroxyl proton. Traces through the exchange cross-peaks are plotted at the top of the contour maps. Note the lower intensity of the GlcA(II)OH3 exchange cross-peak relative to the other hydroxyl resonances.

dx.doi.org/10.1021/jp410540d | J. Phys. Chem. B 2014, 118, 482−491

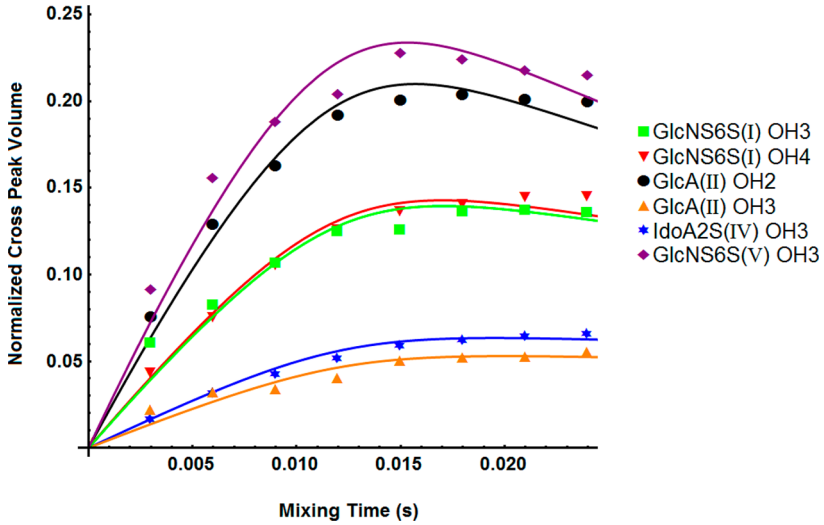

Figure 6. Exchange cross-peak intensity of the Arixtra hydroxyl protons as a function of mixing time. The lower buildup rate observed for the GlcA(II) OH3 and IdoA2S(IV) OH3 protons suggests their involvement in a hydrogen bond consistent with the predictions of the MD simulations in Figure 3.

largest $\Delta\delta$ value, −0.278 ppm, which is consistent with its reduced temperature coefficient and the hydrogen bond predicted by the MD simulations. We also observed a large $\Delta\delta$ value (−0.199 ppm) for GlcNS6S(V) OH3 though the chemical shift of the nonreducing end GlcNS6S(I) OH3 is very close to that of the monosaccharide. As highlighted in Figure 3, the MD simulations predict the GlcNS6S(V) OH3 proton to be involved in a hydrogen bond with the IdoA2S 5O ring oxygen 43% of the time (Table 1). To provide more conclusive evidence of hydrogen bonding, we turned to differences in the rates of chemical exchange of the hydroxyl protons with water.

Arixtra Hydroxyl Proton−Water Chemical Exchange. Chemical exchange of the sugar hydroxyl and water protons produces prominent exchange cross-peaks in the EXSY spectra of oligosaccharides in aqueous solution. Examination of the relative intensities of the exchange cross-peaks of the Arixtra hydroxyl-proton resonances, shown in Figure 5, suggests differences in their solvent exchange rates, especially for GlcA(II)OH3 which gives rise to a much weaker cross-peak than the other hydroxyl groups. Exchange rates were extracted from the buildup curves (Figure 6) for each of the Arixtra hydroxyl protons by nonlinear least-squares fitting to eq 5 and are summarized in Table 2. In these fits, T_{RD} and t_0 were first independently determined for each sample through inversion-recovery experiments (e.g., Figure 1B) on the sample's water resonance, fit to eq 2. The largest exchange rates were measured for GlcA(II) OH2 (22.6 s^{-1}) and GlcNS6S(V) OH3 (25.9 s^{-1}), whereas intermediate rates were observed for the nonreducing end GlcNS6S(I) OH3 (13.8 s^{-1}) and OH4 (14.2 s^{-1}). Although the large $\Delta\delta$ value (−0.199 ppm) for GlcNS6S(V) OH3 and the MD simulation suggested partial involvement of this hydroxyl proton in a hydrogen bond, this is not supported by the exchange rate. In an MD study of factors influencing the conformational preference of the IdoA2S residue, Pol-Fachin and Verli also indicated the presence of a hydrogen bond in IdoA2S(1 → 4)GlcNS6S disaccharides between the OH3 of the GlcNS6S residue and the IdoA2S residue's ring oxygen in both IdoA2S conformations as predicted in this work.[62] The GlcA(II) OH3 and IdoA2S(IV) OH3 hydroxyl protons have the lowest exchange rate constants at 4.72 and 5.73 s^{-1}, respectively. The small exchange rate constant along with the reduced temperature coefficient and $\Delta\delta$ value together provide strong evidence for a GlcA(II) OH3 hydrogen bond, which was predicted in 88% of the structures calculated in the MD simulations. The low exchange rate measured for the IdoA(IV) OH3 hydroxyl proton also suggests that it might be involved in a hydrogen bond despite its larger temperature coefficient. The MD simulations indicate that the IdoA2S(IV) OH3 is involved in a hydrogen bond roughly 51% of the time, switching between the GlcNS3S6S and IdoA2S sulfate groups, which again might explain its higher temperature coefficient.

In summary, the two strongest hydroxyl hydrogen bonds in Arixtra were found to involve the GlcA(II) OH3 and IdoA2S(IV) OH3 protons, demonstrating the importance of these residues in stabilizing a subset of conformations for Arixtra in solution. Thus, in addition to the important role of intermolecular hydrogen bonding to the GlcA carboxyl group in the complex between Arixtra and AT-III,[22,63] we hypothesize that intramolecular hydrogen bonding to GlcA plays an important role in stabilizing the secondary structure of Arixtra, potentially preorganizing it for binding to AT-III. Similarly, it is thought that the participation of the IdoA2S(IV) residue in a hydroxyl-proton hydrogen bond helps to shift the conformational distribution in solution toward ^2S_O, again favoring those structures that are predisposed to bind to AT-III.[23,64]

CONCLUSIONS

This work provides the first experimental evidence for intramolecular hydrogen bonds involving the hydroxyl protons in a heparin oligosaccharide. Hydroxyl hydrogen bonds were identified by the use of exchange rates taken together with temperature coefficient and $\Delta\delta$ measurements. These results highlight the power of MD simulations, which predicted the existence of the GlcA OH3 and IdoA2S OH3 hydrogen bonds, stimulating the experiments described herein, and indicate the hydrogen-bond acceptors. To our knowledge, this is also the first work to address the issue of radiation damping in aqueous solutions when extracting solvent exchange rates of hydroxyl protons.

ASSOCIATED CONTENT

Supporting Information

MD simulation results for the average dihedral angles of Arixtra and Cremer−Pople plots for all five rings of Arixtra. NMR spectra of Arixtra measured as a function of pH. Experimental

dx.doi.org/10.1021/jp410540d | J. Phys. Chem. B 2014, 118, 482−491

details and spectra used for the assignment of the hydroxyl protons of Arixtra. This material is available free of charge via the Internet at http://pubs.acs.org.

AUTHOR INFORMATION

Corresponding Authors

*E-mail leonard.mueller@ucr.edu. Phone: 951-827-3565. Fax: 951-827-4713.

*E-mail: clarive@ucr.edu. Phone: 951-827-2990. Fax: 951-827-4713.

Notes

The authors declare no competing financial interest.

ACKNOWLEDGMENTS

This work was supported by the National Science Foundation (Grants CHE-1213845 to C.K.L. and CHE-0848607 to L.J.M.). C.N.B. acknowledges support from a UCR GRMP fellowship and U.S. Department of Education GAANN Award #P200A120170. R.P.Y. acknowledges support through NSF GRFP Award DGE-0813967.

REFERENCES

(1) Multhaupt, H. A. B.; Couchman, J. R. Heparan Sulfate Biosynthesis: Methods for Investigation of the Heparanosome. *J. Histochem. Cytochem.* **2012**, *60*, 908−915.

(2) Capila, I.; Linhardt, R. J. Heparin−Protein Interactions. *Angew. Chem., Int. Ed.* **2002**, *41*, 391−412.

(3) Jones, C. J.; Beni, S.; Limtiaco, J. F. K.; Langeslay, D. J.; Larive, C. K. Heparin Characterization: Challenges and Solutions. *Annu. Rev. Anal. Chem.* **2011**, *4*, 439−465.

(4) Ornitz, D. M.; Yayon, A.; Flanagan, J. G.; Svahn, C. M.; Levi, E.; Leder, P. Heparin is Required for Cell-Free Binding of Basic Fibroblast Growth Factor to a Soluble Receptor for Mitogenesis in Whole Cells. *Mol. Cell. Biol.* **1992**, *12*, 240−247.

(5) Faham, S.; Hileman, R. E.; Fromm, J. R.; Linhardt, R. J.; Rees, D. C. Heparin Structure and Interactions with Basic Fibroblast Growth Factor. *Science* **1996**, *271*, 1116−1120.

(6) Goodger, S. J.; Robinson, C. J.; Murphy, K. J.; Gasiunas, N.; Harmer, N. J.; Blundell, T. L.; Pye, D. A.; Gallagher, J. T. Evidence That Heparin Saccharides Promote FGF2 Mitogenesis through Two Distinct Mechanisms. *J. Biol. Chem.* **2008**, *283*, 13001−13008.

(7) Zhao, W. J.; McCallum, S. A.; Xiao, Z. P.; Zhang, F. M.; Linhardt, R. J. Binding Affinities of Vascular Endothelial Growth Factor (VEGF) for Heparin-Derived Oligosaccharides. *Biosci. Rep.* **2012**, *32*, 71−81.

(8) Houck, K. A.; Leung, D. W.; Rowland, A. M.; Winer, J.; Ferrara, N. Dual Regulation of Vascular Endothelial Growth Factor Bioavailability by Genetic and Proteolytic Mechanisms. *J. Biol. Chem.* **1992**, *267*, 26031−26037.

(9) Ruhrberg, C.; Gerhardt, H.; Golding, M.; Watson, R.; Ioannidou, S.; Fujisawa, H.; Betsholtz, C.; Shima, D. T. Spatially Restricted Patterning Cues Provided by Heparin-Binding VEGF-A Control Blood Vessel Branching Morphogenesis. *Genes Dev.* **2002**, *16*, 2684−2698.

(10) Jee, J. P.; Nam, S. H.; Park, Y.; Lee, H. J.; Maeng, H. J.; Kim, C. K. Simplified Analysis of Lipoprotein Lipase Activity: Evaluation of Lipasemic Activity of Low Molecular Weight Heparin in Rats. *Arch. Pharm. Res.* **2012**, *35*, 1107−1114.

(11) Spillmann, D.; Lookene, A.; Olivecrona, G. Isolation and Characterization of Low Sulfated Heparan Sulfate Sequences with Affinity for Lipoprotein Lipase. *J. Biol. Chem.* **2006**, *281*, 23405−23413.

(12) van Barlingen, H.; Kleinveld, H. A.; Erkelens, D. W.; deBruin, T. W. A. Lipoprotein Lipase-Enhanced Binding of Lipoprotein(a) [Lp(a)] to Heparan Sulfate Is Improved by Apolipoprotein E (apoE) Saturation: Secretion−Capture Process of ApoE Is a Possible Route for the Catabolism of Lp(a). *Metabolism* **1997**, *46*, 650−655.

(13) Mummery, R. S.; Rider, C. C. Characterization of the Heparin-binding Properties of IL-6. *J. Immunol.* **2000**, *165*, 5671−5679.

(14) Zhang, S. Y.; Condac, E.; Qiu, H.; Jiang, J. L.; Gutierrez-Sanchez, G.; Bergmann, C.; Handel, T.; Wang, L. C. Heparin-Induced Leukocytosis Requires 6-*O*-Sulfation and Is Caused by Blockade of Selectin- and CXCL12 Protein-Mediated Leukocyte Trafficking in Mice. *J. Biol. Chem.* **2012**, *287*, 5542−5553.

(15) Ziarek, J. J.; Veldkamp, C. T.; Zhang, F. M.; Murray, N. J.; Kartz, G. A.; Liang, X. L.; Su, J. D.; Baker, J. E.; Linhardt, R. J.; Volkman, B. F. Heparin Oligosaccharides Inhibit Chemokine (CXC Motif) Ligand 12 (CXCL12) Cardioprotection by Binding Orthogonal to the Dimerization Interface, Promoting Oligomerization, and Competing with the Chemokine (CXC Motif) Receptor 4 (CXCR4) N Terminus. *J. Biol. Chem.* **2013**, *288*, 737−746.

(16) Rosenberg, R. D. Chemistry of Hemostatic Mechanism and Its Relationship to Action of Heparin. *Fed. Proc.* **1977**, *36*, 10−18.

(17) Olson, S. T. Transient Kinetics of Heparin-Catalyzed Protease Inactivation by Antithrombin III. Linkage of Protease Inhibitor Heparin Interactions in the Reaction with Thrombin. *J. Biol. Chem.* **1988**, *263*, 1698−1708.

(18) Thunberg, L.; Backstrom, G.; Lindahl, U. Further Characterization of the Antithrombin-Binding Sequence in Heparin. *Carbohydr. Res.* **1982**, *100*, 393−410.

(19) Atha, D. H.; Lormeau, J. C.; Petitou, M.; Rosenberg, R. D.; Choay, J. Contribution of Monosaccharide Residues in Heparin Binding to Antithrombin III. *Biochemistry* **1985**, *24*, 6723−6729.

(20) Ferro, D. R.; Provasoli, A.; Ragazzi, M.; Torri, G.; Casu, B.; Gatti, G.; Jacquinet, J. C.; Sinay, P.; Petitou, M.; Choay, J. Evidence for Conformational Equilibrium of the Sulfated L-Iduronate Residue in Heparin and in Synthetic Heparin Mono- and Oligosaccharides: NMR and Force-Field Studies. *J. Am. Chem. Soc.* **1986**, *108*, 6773−6778.

(21) Hricovini, M.; Guerrini, M.; Bisio, A.; Torri, G.; Petitou, M.; Casu, B. Conformation of Heparin Pentasaccharide Bound to Antithrombin III. *Biochem. J.* **2001**, *359*, 265−272.

(22) Johnson, D. J. D.; Li, W.; Adams, T. E.; Huntington, J. A. Antithrombin−S195A Factor Xa-Heparin Structure Reveals the Allosteric Mechanism of Antithrombin Activation. *EMBO J.* **2006**, *25*, 2029−2037.

(23) Langeslay, D. J.; Young, R. P.; Beni, S.; Beecher, C. N.; Mueller, L. J.; Larive, C. K. Sulfamate Proton Solvent Exchange in Heparin Oligosaccharides: Evidence for a Persistent Hydrogen Bond in the Antithrombin-Binding Pentasaccharide Arixtra. *Glycobiology.* **2012**, *22*, 1173−1182.

(24) Vilen, E. M.; Lundqvist, L. C. E.; Jouanneau, D.; Helbert, W.; Sandström, C. NMR Study on Hydroxy Protons of κ- and κ-/μ-Hybrid Carrageenan Oligosaccharides: Experimental Evidence of Hydrogen Bonding and Chemical Exchange Interactions in κ/μ Oligosaccharides. *Biomacromolecules* **2010**, *11*, 3487−3494.

(25) Sandström, C.; Kenne, L. Hydroxy Protons in Structural Studies of Carbohydrates by NMR Spectroscopy. *ACS Symp. Ser.* **2006**, *930*, 114−132.

(26) Vasquez, T. E., Jr.; Bergset, J. M.; Fierman, M. B.; Nelson, A.; Roth, J.; Kahn, S. I.; O'Leary, D. J. Using Equilibrium Isotope Effects to Detect Intramolecular OH/OH Hydrogen Bonds: Structural and Solvent Effects. *J. Am. Chem. Soc.* **2002**, *124*, 2931−2938.

(27) Adams, B.; Lerner, L. Observation of Hydroxyl Protons of Sucrose in Aqueous Solution: No Evidence for Persistent Intramolecular Hydrogen Bonds. *J. Am. Chem. Soc.* **1992**, *114*, 4827−4829.

(28) Poppe, L.; van Halbeek, H. The Rigidity of Sucrose: Just an Illusion? *J. Am. Chem. Soc.* **1992**, *114*, 1092−1094.

(29) Battistel, M. D.; Pendrill, R.; Widmalm, G.; Freedberg, D. I. Direct Evidence for Hydrogen Bonding in Glycans: A Combined NMR and Molecular Dynamics Study. *J. Phys. Chem. B* **2013**, *117*, 4860−4869.

(30) Battistel, M. D.; Shangold, M.; Trinh, L.; Shiloach, J.; Freedberg, D. I. Evidence for Helical Structure in a Tetramer of α2-8 Sialic Acid: Unveiling a Structural Antigen. *J. Am. Chem. Soc.* **2012**, *134*, 10717−10720.

(31) Sandström, C.; Baumann, H.; Kenne, L. NMR Spectroscopy of Hydroxy Protons of 3,4-Disubstituted Methyl α-D-Galactopyranosides in Aqueous Solution. *J. Chem. Soc. Perk. T. 2.* **1998**, 809−815.

(32) Dobson, C. M.; Lian, L. Y.; Redfield, C.; Topping, K. D. Measurement of Hydrogen Exchange Rates Using 2D NMR Spectroscopy. *J. Magn. Reson.* **1986**, *69*, 201−209.
(33) Chen, J. H.; Mao, X. A. Measurement of Chemical Exchange Rate Constants with Solvent Protons Using Radiation Damping. *J. Magn. Reson.* **1998**, *131*, 358−361.
(34) Pedretti, A.; Villa, L.; Vistoli, G. VEGA: A Versatile Program to Convert, Handle and Visualize Molecular Structure on Windows-Based PCs. *J. Mol. Graph. Model.* **2002**, *21*, 47−49.
(35) Case, D. A., Darden, T. A., Cheatham III, T. E., Simmerling, C. L., Wang, J., Duke, R. E., Luo, R., Walker, R. C., Zhang, W., Merz, K. M., et al. 2011, AMBER 11.
(36) Kirschner, K. N.; Yongye, A. B.; Tschampel, S. M.; Gonzalez-Outeirino, J.; Daniels, C. R.; Foley, B. L.; Woods, R. J. GLYCAM06: A Generalizable Biomolecular Force Field. Carbohydrates. *J. Comput. Chem.* **2008**, *29*, 622−655.
(37) Hornak, V.; Abel, R.; Okur, A.; Strockbine, B.; Roitberg, A.; Simmerling, C. Comparison of Multiple Amber Force Fields and Development of Improved Protein Backbone Parameters. *Proteins* **2006**, *65*, 712−725.
(38) Jorgensen, W. L.; Chandrasekhar, J.; Madura, J. D.; Impey, R. W.; Klein, M. L. Comparison of Simple Potential Functions for Simulating Liquid Water. *J. Chem. Phys.* **1983**, *79*, 926−935.
(39) Phillips, J. C.; Braun, R.; Wang, W.; Gumbart, J.; Tajkhorshid, E.; Villa, E.; Chipot, C.; Skeel, R. D.; Kale, L.; Schulten, K. Scalable Molecular Dynamics with NAMD. *J. Comput. Chem.* **2005**, *26*, 1781−1802.
(40) Darden, T.; York, D.; Pedersen, L. Particle Mesh Ewald: An *N*·log(*N*) Method for Ewald Sums in Large Systems. *J. Chem. Phys.* **1993**, *98*, 10089−10092.
(41) Miyamoto, S.; Kollman, P. A. SETTLE: An Analytical Version of the SHAKE and RATTLE Algorithm for Rigid Water Models. *J. Comput. Chem.* **1992**, *13*, 952−962.
(42) Humphrey, W.; Dalke, A.; Schulten, K. VMD: Visual Molecular Dynamics. *J. Mol. Graph. Model.* **1996**, *14*, 33−38.
(43) Forster, M. J. *mdxvu − molecular dynamics X11 viewer*; 2008; available at http://sourceforge.net/projects/mdxvu/ (accessed 01/04/2014).
(44) Ragazzi, M.; Ferro, D. R.; Perly, B.; Torri, G.; Casu, B.; Sinay, P.; Petitou, M.; Choay, J. Conformation of the Pentasaccharide Corresponding to the Binding Site of Heparin to Antithrombin III. *Carbohydr. Res.* **1987**, *165*, C1−C5.
(45) Ragazzi, M.; Ferro, D. R.; Perly, B.; Sinay, P.; Petitou, M.; Choay, J. Conformation of the Pentasaccharide Corresponding to the Binding Site of Heparin for Antithrombin III. *Carbohydr. Res.* **1990**, *195*, 169−185.
(46) Hwang, T. L.; Shaka, A. J. Water Suppression That Works. Excitation Sculpting Using Arbitrary Wave Forms and Pulsed Field Gradients. *J. Magn. Reson. Ser. A* **1995**, *112*, 275−279.
(47) Langeslay, D. J.; Beecher, C. N.; Dinges, M. M.; Larive, C. K. Glycosaminoglycan Structural Characterization. *eMagRes* **2013**, *2*, 205−214.
(48) Van Geet, A. L. Calibration of Methanol and Glycol Nuclear Magnetic Resonance Thermometers with a Static Thermistor Probe. *Anal. Chem.* **1968**, *40*, 2227−2229.
(49) Jeener, J.; Meier, B. H.; Bachmann, P.; Ernst, R. R. Investigation of Exchange Processing by 2-Dimensional NMR Spectroscopy. *J. Chem. Phys.* **1979**, *71*, 4546−4553.
(50) Bloembergen, N.; Pound, R. V. Radiation Damping in Magnetic Resonance Experiments. *Phys. Rev.* **1954**, *95*, 8−12.
(51) Szoke, A.; Meiboom, S. Radiation Damping in Nuclear Magnetic Resonance. *Phys. Rev.* **1959**, *113*, 585−586.
(52) Chen, J. H.; Cutting, B.; Bodenhausen, G. Measurement of Radiation Damping Rate Constants in Nuclear Magnetic Resonance by Inversion Recovery and Automated Compensation of Selective Pulses. *J. Chem. Phys.* **2000**, *112*, 6511−6514.
(53) Chen, J. H.; Mao, X. A. Radiation Damping Transfer in Nuclear Magnetic Resonance Experiments via Chemical Exchange. *J. Chem. Phys.* **1997**, *107*, 7120−7126.
(54) Berger, S.; Braun, S. *200 and More NMR Experiments: A Practical Course*, 3rd ed.; Wiley-VCH: Weinheim, Germany, 2004.
(55) Wolfram, S. *Mathematica: A System for Doing Mathematics by Computer*, 2nd ed.; Addison-Wesley Publishing Company: Reading, MA, 1991.
(56) Abramowitz, M.; Stegun, I. A. *Handbook of Mathematical Functions with Formulas, Graphs, and Mathematical Tables*; U.S. Government Printing Office: Washington, D.C., 1964.
(57) Langeslay, D. J.; Beni, S.; Larive, C. K. Detection of the ^{1}H and ^{15}N NMR Resonances of Sulfamate Groups in Aqueous Solution: A New Tool for Heparin and Heparan Sulfate Characterization. *Anal. Chem.* **2011**, *83*, 8006−8010.
(58) Langeslay, D. J.; Beecher, C. N.; Naggi, A.; Guerrini, M.; Torri, G.; Larive, C. K. Characterizing the Microstructure of Heparin and Heparan Sulfate Using *N*-Sulfoglucosamine ^{1}H and ^{15}N NMR Chemical Shift Analysis. *Anal. Chem.* **2013**, *85*, 1247−1255.
(59) Baxter, N. J.; Williamson, M. P. Temperature Dependence of ^{1}H Chemical Shifts in Proteins. *J. Biomol. NMR* **1997**, *9*, 359−369.
(60) Kindahl, L.; Sandström, C.; Norberg, T.; Kenne, L. ^{1}H NMR Studies of Hydroxy Protons of Asn- and Ser-Linked Disaccharides in Aqueous Solution. *J. Carbohydr. Chem.* **2000**, *19*, 1291−1303.
(61) Kindahl, L.; Sandström, C.; Norberg, T.; Kenne, L. ^{1}H NMR Studies of Hydroxy Protons of the V[*β*-Gal(1→3)-*α*-GalNAc(1→O)]THPGY Glycopeptide. *Carbohydr. Res.* **2001**, *336*, 319−323.
(62) Pol-Fachin, L.; Verli, H. Depiction of the Forces Participating in the 2-*O*-Sulfo-*α*-L-iduronic Acid Conformational Preference in Heparin Sequences in Aqueous Solutions. *Carbohydr. Res.* **2008**, *343*, 1435−1445.
(63) van Boeckel, C. A. A.; Petitou, M. The Unique Antithrombin III Binding Domain of Heparin: A Lead to New Synthetic Antithrombotics. *Angew. Chem., Int. Ed.* **1993**, *32*, 1671−1690.
(64) Guerrini, M.; Elli, S.; Gaudesi, D.; Torri, G.; Casu, B.; Mourier, P.; Herman, F.; Boudier, C.; Lorenz, M.; Viskov, C. Effects on Molecular Conformation and Anticoagulant Activities of 1,6-Anhydrosugars at the Reducing Terminal of Antithrombin-Binding Octasaccharides Isolated from Low-Molecular-Weight Heparin Enoxaparin. *J. Med. Chem.* **2010**, *53*, 8030−8040.